Climate Transition Zones as Emerging Hotspots for Natural Hazards: Insights from Land Use- Climate Feedbacks Amplify Disaster Risk in Taiwan

Manikandan Sathianarayanan [1,2], Pai-Hui Hsu [3]

[1] Department of Civil Engineering, National Taiwan University, Taiwan – d06521026@ntu.edu.tw
[2] Research Centre for Humanities and Social Sciences (RCHSS), Academia Sinica, Taiwan.
[3] Department of Civil Engineering, National Taiwan University, Taiwan – hsuph@ntu.edu.tw

Keywords: LULC change, KG climate zone change, Spatial co-occurrence, Natural disaster.

Abstract

Human-driven land use change and global climate variability are jointly reshaping regional environmental processes, yet their combined influence on climate classification and hazard dynamics remains underexplored. This study integrates satellite-derived land use/land cover (LULC) data, Köppen–Geiger climate classifications derived from CHIRPS precipitation and MODIS land surface temperature, and a disaster inventory (2001–2020) to examine land–climate–hazard interactions in Taiwan. Results indicate notable LULC transitions, including a 0.98% increase in woody savannas and a 0.72% decline in wetlands, coinciding with a significant expansion of tropical climate zones (Aw +14,172 km²; Af +1,038 km²) and a contraction of temperate regions (−15,365 km²). Approximately 68% of observed LULC changes spatially correspond with shifting climate zones, suggesting strong land–climate coupling. Transition zones, covering only 15% of Taiwan's land area, exhibit disaster frequencies 2.8 times higher than stable regions. Warming transition areas account for over half of typhoon-induced landslides and a substantial proportion of major flood events in recent years. Localized warming exceeding 1°C is closely linked to albedo reduction from deforestation, while intensified precipitation extremes correlate with agricultural expansion ($r = 0.73$). These findings highlight climate transition zones as emerging hazard hotspots and underscore the need for dynamic, climate-informed land-use planning strategies.

1. Introduction

Anthropogenic climate change is intensifying hydro-meteorological extremes and reshaping regional climate regimes (Yilmaz, 2016). The IPCC Sixth Assessment Report highlights increasing risks of extreme rainfall, tropical cyclones, and compound hazards under continued warming (Intergovernmental Panel on Climate, 2023). In Taiwan, interactions between monsoon circulation, diurnal convection, and typhoon activity have amplified rainfall intensity, elevating flood and landslide susceptibility (Huang et al., 2016). Combined with its active arc–continent collision setting and steep topography, Taiwan experiences frequent multi-hazard events, making it highly vulnerable to climate-driven geohazards (Tsou et al., 2011).

Beyond atmospheric forcing, anthropogenic land use/land cover (LULC) change—such as deforestation, agricultural expansion, and infrastructure development—alters vegetation structure, soil cohesion, hydrological response, and surface energy balance (Vuillez et al., 2018). Emerging research indicates bidirectional coupling between LULC transformations and Köppen–Geiger (KG) climate zone shifts, where land modification influences regional climatic feedbacks while climate migration reshapes ecosystem stability (Malone, 2023). Transition (ecotonal) climate zones are particularly sensitive to hydrothermal variability and may function as emerging risk hotspots under compounded warming and land disturbance (Santos et al., 2025).

Despite extensive studies in Taiwan on typhoon-induced landslides, precipitation trends, and flood hazards, disaster mechanisms linked explicitly to shifting climate zones remain largely unexplored (Yang et al., 2015). Most hazard assessments assume static climatic baselines and do not account for spatial reclassification of climate regimes over time. This limitation constrains understanding of how evolving climate boundaries interact with human land-use decisions to amplify hazard frequency (Hurlbert et al., 2019).

This study investigates two key questions: (1) whether LULC changes contribute to regional KG climate zone shifts, and (2) whether such shifts intensify disaster occurrence. By integrating satellite-derived LULC data, climate classifications derived from CHIRPS precipitation and MODIS land surface temperature, and a multi-year disaster inventory, we develop a spatially explicit framework to quantify land–climate–hazard interactions in Taiwan. The results aim to advance dynamic risk assessment approaches and support climate-informed land-use planning in rapidly transforming environments.

2. Materials and methods

2.1 Study area

The study area is Taiwan, located in East Asia along the western Pacific Ocean, including the main island and surrounding offshore islands (Fig. 1a). The island is bordered by the Pacific Ocean to the east, the Bashi Channel to the south, the Taiwan Strait to the west, and the East China Sea to the north. It extends between 120°E–122°E and 22°N–25°N, covering approximately 36,197 km². Taiwan is about 394 km long (north–south) and 144 km wide (west–east), with steep mountain ranges dominating the eastern region and gently sloping plains in the west.
Taiwan has a subtropical to tropical climate, with an average annual temperature of about 22°C and mean annual precipitation of roughly 2500 mm (Sathianarayanan and Hsu, 2026). Temperature seasonality is stronger in the north (15.0°C in January to 28.7°C in July) than in the south (18.2°C to 28.4°C). Precipitation shows strong spatial variability, with

higher rainfall in mountainous and eastern regions and lower totals in western lowlands. Annual rainfall ranges from approximately 1500 mm in southwestern Taiwan to over 6500 mm in northeastern mountainous areas.

The dataset includes landslides triggered by typhoons and extreme rainfall, as well as documented flood occurrences.

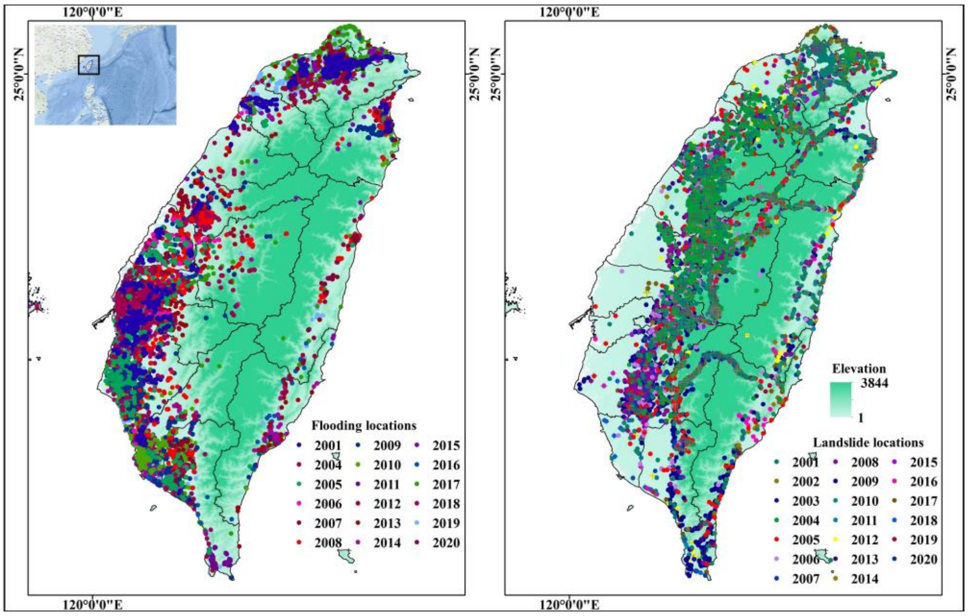

Fig 1. Study area with disaster occurrence locations

2.2 Dataset used for this study

2.2.1 Satellite data

This study utilized time-series MODIS vegetation index data at 1 km spatial resolution with monthly intervals from February 2000 to December 2020. A total of 964 images were obtained from the Land Processes Distributed Active Archive Center (LP DAAC). The dataset was generated using the constrained view maximum value compositing method to reduce cloud and atmospheric effects. Preprocessing included HDF-to-GeoTIFF conversion, reprojection from the sinusoidal system to WGS84/Albers Equal Area Conic, and band extraction using the MODIS Reprojection Tool (MRT). To further reduce cloud contamination and remove noise, the Savitzky–Golay filtering algorithm was applied in TIMESAT (Sathianarayanan and Hsu, 2023).

Land Surface Temperature (LST) data were derived from MODIS Terra and Aqua sensors at 1 km resolution for 2000–2020. Terra and Aqua provide complementary overpass times, enabling consistent daytime observations. The MOD11A1 daytime LST product was retrieved from the USGS Earth Explorer platform. LST retrieval is based on the split-window algorithm using thermal infrared bands 31 and 32, correcting for atmospheric effects and surface emissivity variations (Hsu et al., 2025).

Precipitation data were obtained from the CHIRPS dataset (2000–2020), developed by the Climate Hazards Group (UCSB). CHIRPS provides near–real-time precipitation estimates at 0.05° (~5 km) resolution between 50°S–50°N. The dataset integrates infrared cold cloud duration observations, TRMM-based calibration, and in-situ station measurements to improve accuracy, particularly in regions with complex topography and convective precipitation systems.

2.2.2 Disaster inventory dataset

A disaster inventory was compiled to analyse landslide and flood events across Taiwan from 2001 to 2020.

Landslide records were obtained from multiple government agencies, including the Ministry of the Interior, Forest Bureau, National Science and Technology Centre for Disaster Reduction (NCDR), Water Resources Agency (WRA), Highway Bureau, and fire departments. A total of 11,376 landslide locations were documented, with the WRA and Highway Bureau contributing the majority of records. Flood data were collected from city governments, fire departments, NCDR, the Emergency Management Information System (EMIS), and WRA, resulting in 14,148 recorded flood locations. All events included documented infrastructure damage and were verified through field investigations and high-resolution satellite imagery. Although an NDVI-based landslide inventory derived from Formosat-2 imagery exists, its susceptibility to misclassification in shadowed terrain reduced reliability. Therefore, this study relies exclusively on official, field-verified government datasets to ensure spatial accuracy and consistency.

2.3 Framework for this study

This study employs an integrated analytical framework to investigate the cascading relationships between land use/land cover (LULC) change, climate zone shifts, and disaster occurrence in Taiwan from 2001 to 2020. The methodology comprises four sequential stages, as illustrated in Figure 2.

First, multi-source satellite data, including MODIS-derived land cover and land surface temperature (LST) and CHIRPS precipitation, were processed and integrated with a comprehensively validated disaster inventory. Second, inter-annual change detection using image differencing was applied to generate precise time-series of LULC and Köppen-Geiger (KG) climate zone transitions. The core of the analysis involved, third, a spatial co-occurrence analysis to quantify the overlap between LULC change boundaries and KG zone transitions. Finally, this framework enabled the modelling of disaster risk by correlating the identified climate transition zones with the historical locations of landslides and floods. This end-to-end process provides a robust mechanism for linking anthropogenic environmental changes to evolving hazard patterns.

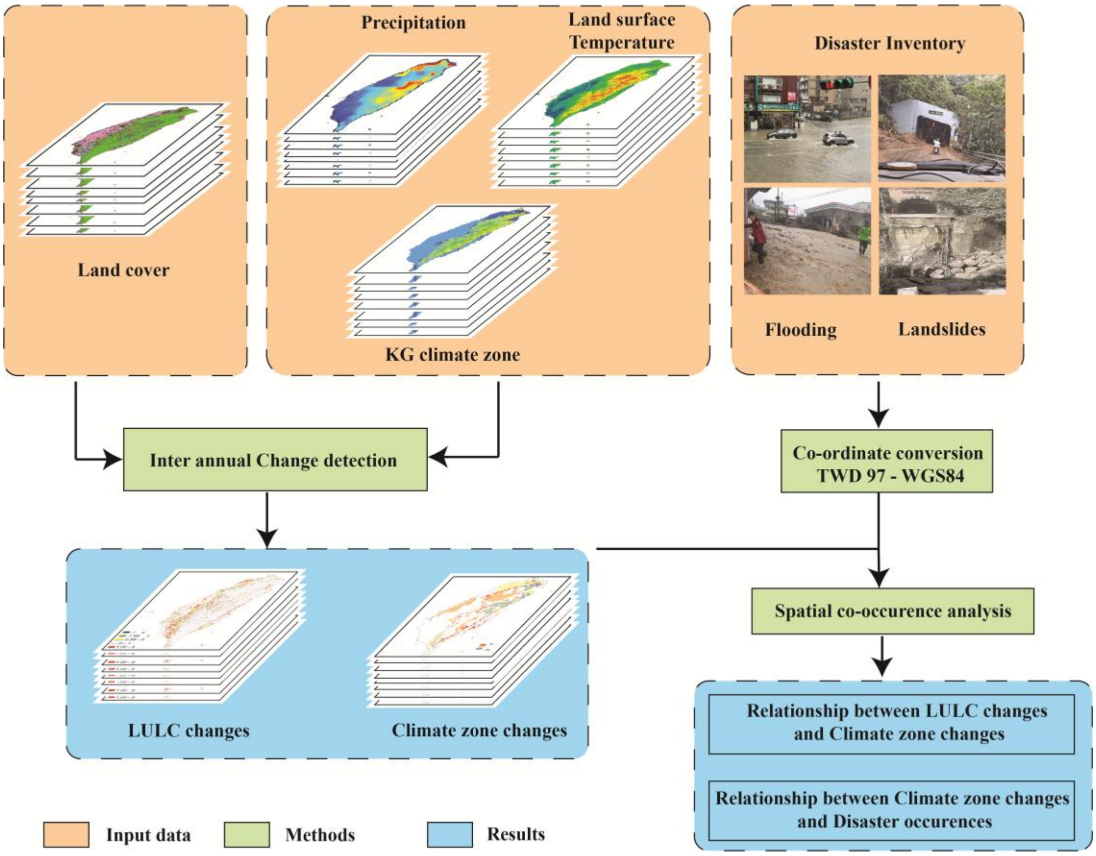

Fig 2. Methodology adopted for this study

2.3.1 Koppen-Geiger Climate classification

The Köppen–Geiger climate classification (KGC) system categorizes global climates based on long-term monthly temperature and precipitation patterns. It defines five major climate groups: tropical (A), arid (B), temperate (C), cold/snow (D), and polar (E). Arid climates are distinguished by precipitation–evapotranspiration balance, while the remaining groups are primarily determined by temperature thresholds and seasonal variability. Key boundaries are defined using mean monthly temperature criteria. Tropical (A) and temperate (C) climates are separated by a +18 °C coldest-month mean temperature. Temperate (C) and cold (D) climates are distinguished by a −3 °C threshold for the coldest month, and cold (D) and polar (E) climates are divided by a +10 °C warmest-month mean temperature.

2.3.2 Spatial–Temporal Change Detection

Land cover and climate zone changes were quantified using pixel-level image differencing:

$$I_d(x,y) = I_1(x,y) - I_2(x,y) \tag{1}$$

Where I_1 and I_2 = co-registered images from two time periods
I_d = pixel-wise difference.

Land cover dynamics were derived from the MODIS MCD12Q1 (LC_Type1) product based on the IGBP 17-class scheme. Data preprocessing included mosaicking and reprojection from the sinusoidal to a geographic coordinate system using the MODIS Reprojection Tool.

Climate zones were mapped using the Köppen–Geiger framework. Monthly precipitation (CHIRPS) and monthly mean temperature aggregated from MOD11A1 LST were used to compute key climatic variables, including mean annual temperature and precipitation. These variables enabled pixel-level classification into KG subclasses and major climate groups. Final maps were exported as georeferenced GeoTIFFs. Annual KG maps were generated for 2001–2020 in MATLAB. Interannual changes were detected by subtracting consecutive yearly maps, producing 19 difference layers (2001–2002 to 2019–2020). This sequential approach captures year-to-year variability and avoids information loss associated with conventional baseline–endpoint comparisons.

2.3.3 Spatial co-occurrence analysis

Spatial co-occurrence analysis was conducted in ArcGIS to (1) quantify the relationship between land-use/land-cover (LULC) changes and climate zone transitions, and (2) examine associations between climate zone shifts and disaster events. Following established overlap statistics, direct spatial coincidence between two variables was measured using boundary intersections:

$$O_s = card(B_G \cap B_H) \tag{2}$$

Where O_s represents the number of coincident boundary locations between variables G and H.

To further assess spatial lag effects, the mean minimum Euclidean distance between boundary elements was calculated:

$$O_x = \frac{\sum_{i=1}^{N_x} \min(d_i)}{N_x} \tag{3}$$

Where $\min(d_i)$ = shortest distance from the i th boundary element of variable X to variable Y.

N_x = total number of boundary elements in X.
Interannual LULC and climate zone changes were derived from raster-based change detection. Disaster events (landslides and floods) were compiled as point data with associated attributes. Landslide coordinates in TWD97 were converted to WGS84 using Python and imported into ArcGIS. Raster change layers were converted to point features to enable spatial relationship analysis between LULC dynamics, climate transitions, and disaster occurrences across Taiwan.

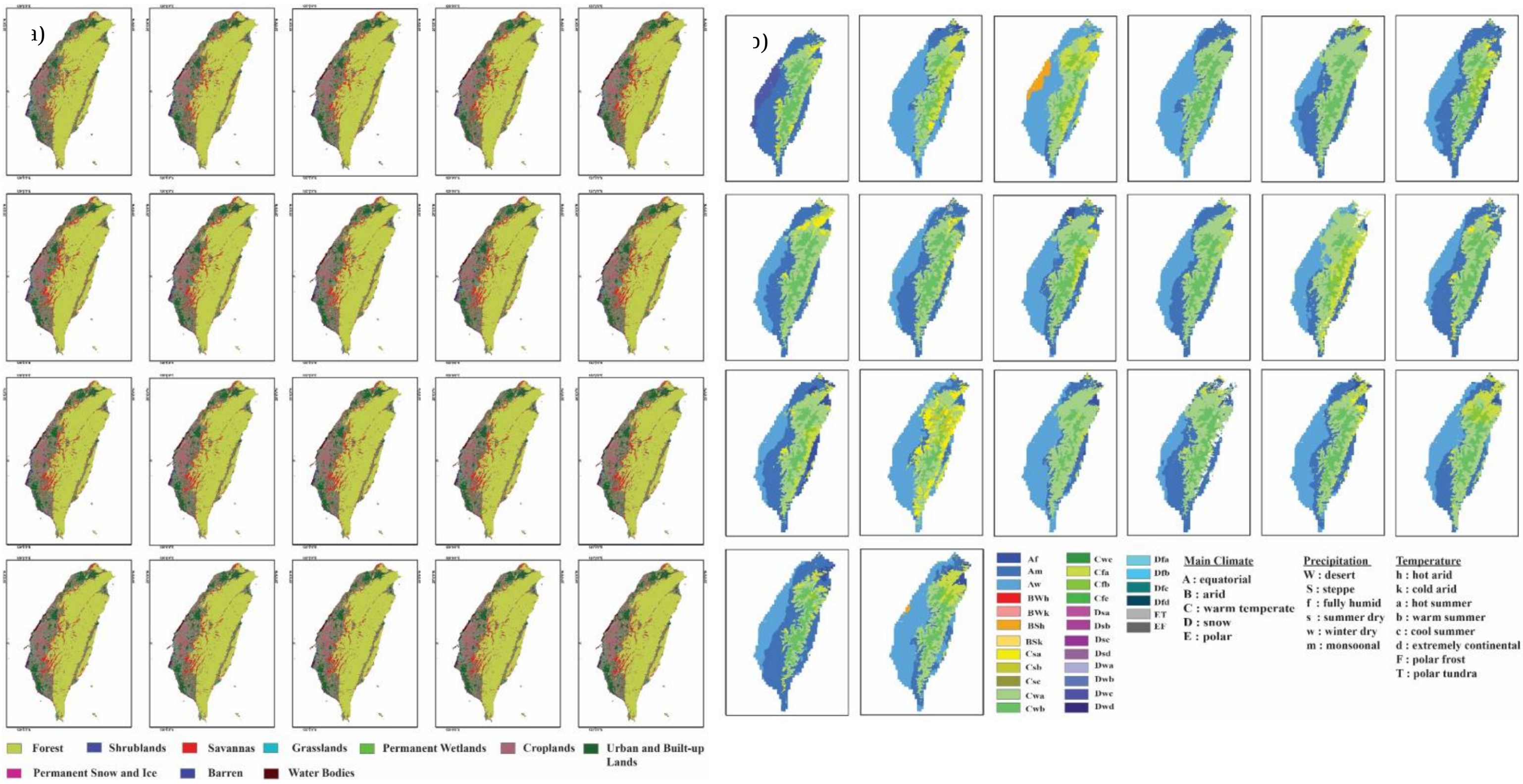

Fig 3. a) land cover changes from 2001-2020 and b) climate zone changes from 2001-2020 (Sathianarayanan and Hsu, 2026).

3. Results and Discussion

3.1 Interannual land cover changes

MODIS land cover maps (Fig.3a) show clear topographic and climatic controls on Taiwan’s LULC patterns: forest dominates the Central Mountain Range and eastern regions, while urban and agricultural land concentrates in western lowlands. In 2020, evergreen broadleaf forest was the largest class (~45%), followed by croplands (~11%) and urban/built-up areas (~8%); several classes (evergreen needleleaf forest, wetlands, woody savannas) each accounted for ~4%. Net LULC change from 2001–2020 indicates expansions in woody savannas (+0.98%), evergreen broadleaf forest (+0.93%), and croplands (+0.70%), while notable declines occurred in savannas (−0.88%), permanent wetlands (−0.72%), and cropland–natural vegetation mosaics (−0.51%) (Table 1). Interannual trajectories varied by class, with different forest types and shrublands showing phase-like fluctuations rather than monotonic trends.

3.2 Interannual Köppen–Geiger climate zone change (2001–2020)

The 2020 Köppen–Geiger (KG) map (Fig. 3b) identifies 10 climate zones (Af, Am, Aw, Cfa, Cfb, Cwa, Cwb, BSh, Csa, Dfa). Aw is dominant (~41%), followed by Cwa (~20%) and Am (~15%); several minor zones (e.g., BSh, Csa, Dfa) occupy very small fractions (<1%). Interannual variability is pronounced, especially over the Central Mountain Range, reflecting elevation-driven microclimatic complexity. The BSh class appears intermittently along western coastal areas (e.g., 2003 and 2020). Between 2001 and 2020, climate zones reorganized substantially (Table 2), including expansion of Af and Cfb and contraction of Am and Csa. Several small-area classes present in early years disappeared by 2020, while others emerged only intermittently with minimal extent.

Table 1. Net LULC area change (2001–2010, 2010–2020, 2001–2020). -ve indicate loss; positive values indicate gain

Category	2001-2010	2010-2020	2001-2020
Evergreen Needleleaf Forests	-82.2	-89.2	-171.5
Evergreen Broadleaf Forests	390.7	-830.7	-440
Deciduous Needleleaf Forests	-80.5	-71.2	-151.7
Deciduous Broadleaf Forests	-132.5	56	-76.5
Mixed Forests	-28.2	74.5	46.2
Closed Shrublands	12.5	15.5	28
Open Shrublands	-5.75	21.7	16
Woody Savannas	-735.2	277	-458.5
Savannas	-426.7	842.5	415.7
Grasslands	-108.5	278.7	170.2
Permanent Wetlands	221.2	115.7	337
Croplands	493.7	-825	-331.2
Urban and Built-up Lands	322	-63.2	258.7
Cropland/Natural Vegetation Mosaics	174.7	63.7	238.5
Permanent Snow and Ice	16.2	4.7	21
Barren	-18.	127.2	108.7
Water Bodies	-13	2	-11

Table 2. Net change in climate zone distribution (pixel counts) for 2001–2010, 2010–2020, and 2001–2020.

Climate Zones	2001-2010	2010-2020	2001-2020
Af	77	2	44
Am	6791	8525	14172
Aw	0	236	218
Csa	1432	313	1497
Csb	330	0	330
Cwa	1149	6123	4445
Cwb	1408	1529	2478
Cfa	645	340	561
Cfb	12	18	10
Dwa	1	0	1
Dwb	3	0	3

3.3 Spatial Distribution of LULC and Climate Zone Changes

Spatial analysis of interannual land use/land cover (LULC) and Köppen–Geiger (KG) climate zone changes was conducted to identify areas of significant transformation and evaluate spatial correspondence between land dynamics and climate transitions. Figure 3 illustrates interannual LULC changes (2001–2020), while Figure 4 presents corresponding KG climate zone shifts.

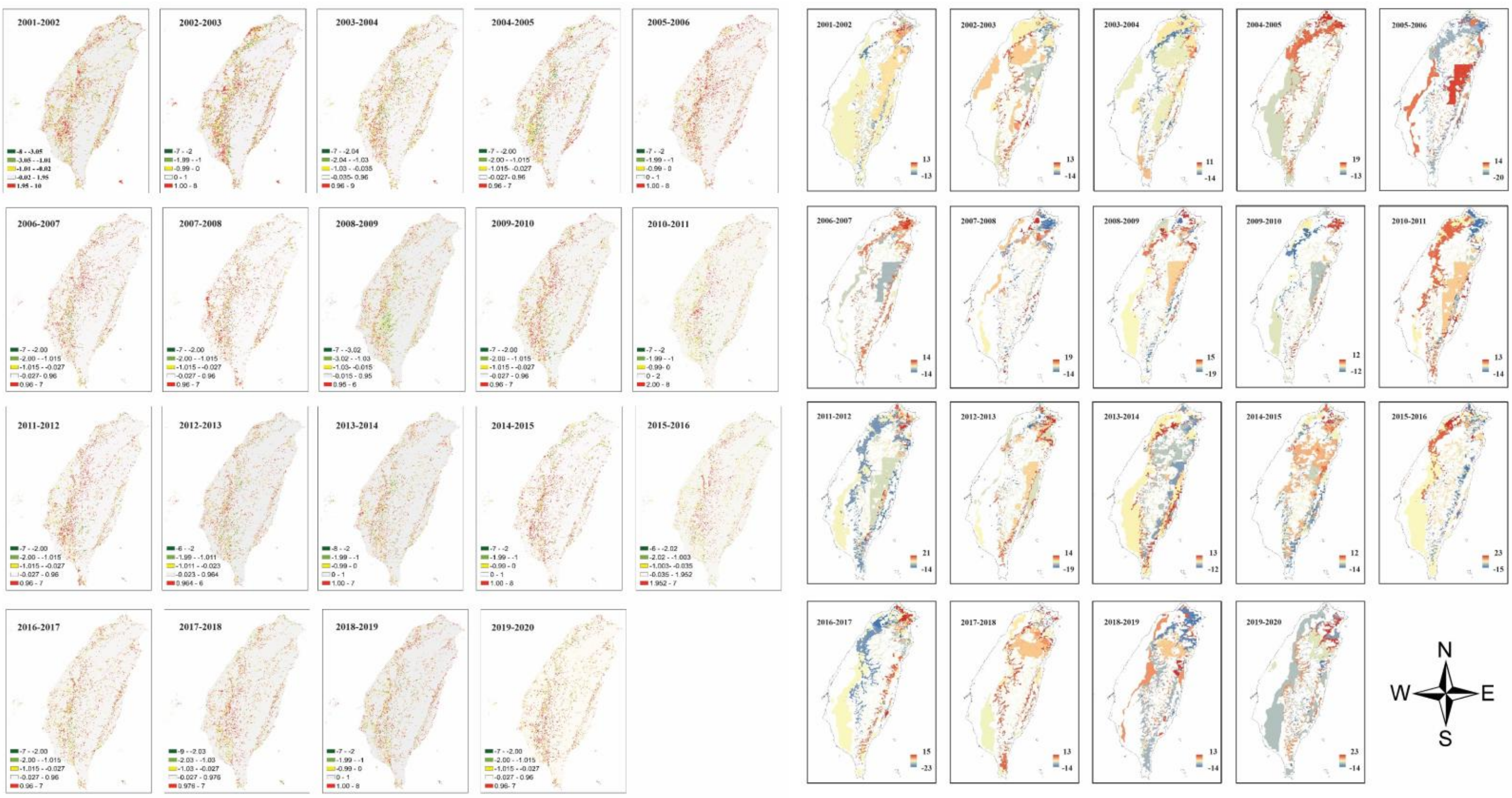

Fig 4.Spatial distribution of a) land cover changes b) climate zone changes (Sathianarayanan and Hsu, 2026).

LULC changes were most pronounced in southwestern Taiwan, extending toward the foothills of the Central Mountain Range, whereas the central mountainous ridge exhibited relatively limited change. Positive LULC transitions were more frequent during the early study period, while later years showed reduced expansion. Negative LULC changes were scattered across southwestern and northern Taiwan, with localized intensification during 2008–2009. Climate zone transitions displayed clear spatial variability, particularly in eastern and northern Taiwan. Positive values represent shifts toward warmer zones, while negative values indicate transitions toward cooler regimes. The most substantial warming-related transitions occurred in 2015–2016 and 2019–2020, whereas 2018–2019 recorded the strongest cooling-related shift (−9.30%). Notably, 2016–2017 exhibited strong bidirectional change (+5.78% vs. −3.20%), suggesting heightened climatic variability. Net percentage analysis (Table 2) reveals alternating phases of expansion and contraction, with recent years showing amplified fluctuations. These findings highlight the dynamic and spatially heterogeneous evolution of Taiwan’s climate zones and land cover patterns, with increasing interannual variability in the late study period.

3.4 Relationship Between LULC Changes and Climate Zone Transitions

Spatial co-occurrence analysis quantified the proportion of LULC changes overlapping with Köppen–Geiger (KG) climate zone transitions. Results reveal substantial interannual variability in spatial correspondence (Fig. 5). In several years, more than 50% of LULC changes coincided with climate zone reclassification, indicating strong coupling. For example, 95.7% of LULC changes in 2001–2002 overlapped with positive (warming) climate transitions. Similarly, 67.1% of LULC changes in 2011–2012 aligned with negative (cooling) transitions.

Conversely, certain years exhibited weak spatial overlap, such as 2003–2004, where only 5.4% of LULC changes corresponded with positive transitions. These low-overlap periods suggest that broader atmospheric drivers may have dominated climate variability. Notable asymmetry was observed: years such as 2001–2002 and 2019–2020 showed strong alignment between LULC change and warming transitions, whereas 2011–2012 displayed stronger correspondence with cooling shifts. This pattern suggests that land cover transformations may contribute to regional warming or drying tendencies under specific conditions.

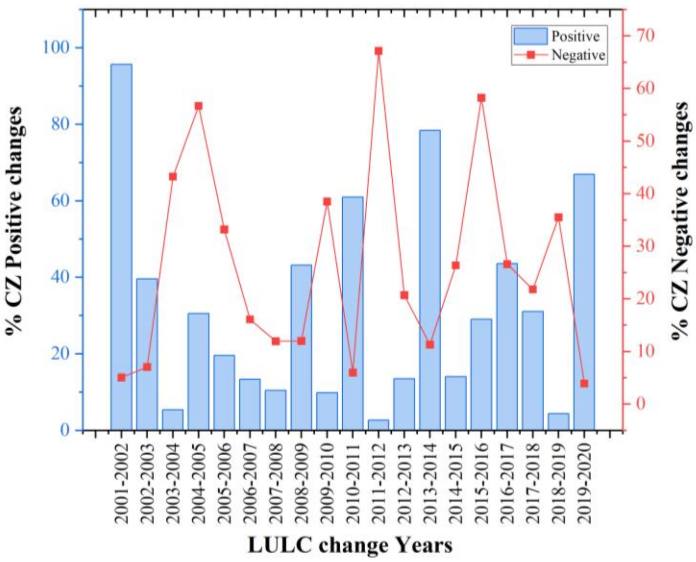

Fig 5. Percentage of lulc changes against climate zone changes (Sathianarayanan and Hsu, 2026)

3.5 Relationship Between Climate Zone Changes and Disasters

Disaster inventories (typhoon-induced landslides, heavy rainfall-induced landslides, and floods) were spatially intersected with climate transition zones in ArcGIS (Table 3). Results show differentiated hazard sensitivities. Typhoon-induced landslides were slightly more frequent in negatively shifting climate zones (58.1% overall), while heavy rainfall-induced landslides showed a modest predominance in negatively transitioned areas. Flood events exhibited the strongest association with positive climate transitions.

During the peak flood year (2017–2018), 83.4% of flood incidents occurred in zones experiencing positive shifts, suggesting intensified moisture regimes. Across all hazard types, areas undergoing climate transitions (both positive and negative) recorded 42% more disaster events than stable regions, highlighting the compounding risks associated with dynamic climate zone migration. These findings demonstrate that climate transition zones function as emerging hazard hotspots and underscore the importance of integrating climate reclassification into dynamic risk assessment frameworks.

4. Conclusion

This study investigates the relationships between land use/land cover (LULC) changes, Köppen–Geiger (KG) climate zone shifts, and disaster occurrence in Taiwan from 2001 to 2020. Results indicate significant LULC transitions, including expansion of woody savannas and evergreen broadleaf forests and reductions in wetlands and croplands, driven by anthropogenic activities and extreme events such as Typhoon Morakot. These land transformations corresponded with climate zone reorganization, characterized by expansion of tropical climates (Af, Aw) and contraction of temperate zones, consistent with regional warming trends.

Although only 15% of Taiwan experienced climate zone transitions, these areas accounted for 42% of recorded disasters, highlighting their elevated vulnerability. Typhoon-induced landslides were 1.7 times more frequent in warming zones, rainfall-induced landslides showed greater occurrence in cooling areas, and 83% of severe floods occurred in regions shifting toward warmer and more humid conditions.

These findings demonstrate that climate transition zones function as emerging hazard hotspots. Integrating dynamic climate classification with land-use planning is therefore essential for adaptive risk management. Future work should incorporate higher-resolution climate modelling and socioeconomic factors to strengthen resilience strategies in Taiwan's rapidly evolving environmental landscape.

Table 3. Association between KG climate zone changes and disaster events

year of changes	Typhoon induced Landslide			Heavy rain induced landslide			Flooding		
	(+) CZ changes	(-) CZ changes	Total points	(+) CZ changes	(-) CZ changes	Total points	(+) CZ changes	(-) CZ changes	Total points
2001-2002	258	93	767	53	6	142	315	62	1144
2002-2003	43	11	149	4	6	17	-	-	-
2003-2004	10	14	50	0	4	15	0	57	398
2004-2005	541	770	1974	43	67	228	28	238	1047
2005-2006	76	238	961	29	30	184	58	7	356
2006-2007	29	50	431	21	24	182	48	5	566
2007-2008	55	50	551	8	11	126	52	86	1054
2008-2009	563	27	1398	0	0	1	232	10	1150
2009-2010	35	504	1586	3	26	150	1	139	1016
2010-2011	86	21	437	80	16	319	15	0	148
2011-2012	10	105	412	2	104	219	25	138	362
2012-2013	29	42	453	5	14	110	17	43	472
2013-2014	172	38	499	12	5	99	69	2	295
2014-2015	15	23	162	23	11	98	61	99	443
2015-2016	47	75	303	7	8	70	0	96	436
2016-2017	36	19	229	51	60	285	389	156	1582
2017-2018	77	3	327	10	33	137	70	186	1923
2018-2019	3	35	166	5	41	106	7	190	1267
2019-2020	58	14	162	19	3	43	164	0	489

References

Hsu, P.-H., Sathianarayanan, M., Gianoli, A., 2025. Maximizing cooling benefits through urban green and blue spaces in Taipei city. Discover Cities 2, 115.

Huang, W.-R., Chang, Y.-H., Hsu, H.-H., Cheng, C.-T., Tu, C.-Y., 2016. Dynamical downscaling simulation and future projection of summer rainfall in Taiwan: Contributions from different types of rain events. Journal of Geophysical Research: Atmospheres 121, 13,973–913,988.

Hurlbert, M., Krishnaswamy, J., Johnson, F.X., Rodríguez-Morales, J.E., Zommers, Z., 2019. Risk Management and Decision making in Relation to Sustainable Development, in: Shukla, P.R., Skea, J., Buendia, E.C., Masson-Delmotte, V., Pörtner, H.O., Roberts, D.C., Zhai, P., Slade, R., Connors, S., Diemen, R.v., Ferrat, M., Haughey, E., Luz, S., Neogi, S., Pathak, M., Petzold, J., Pereira, J.P., Vyas, P., Huntley, E., Kissick, K., Belkacemi, M., Malley, J. (Eds.), Climate Change and Land : an IPCC special report on climate change, desertification, land degradation, sustainable land management, food security, and greenhouse gas fluxes in terrestrial ecosystems. Intergovernmental Panel on Climate Change, pp. 673–800.

Intergovernmental Panel on Climate, C., 2023. Climate Change 2022 – Impacts, Adaptation and Vulnerability: Working Group II Contribution to the Sixth Assessment Report of the Intergovernmental Panel on Climate Change. Cambridge University Press, Cambridge.

Malone, A.G.O., 2023. Quantifying Who Will Be Affected by Shifting Climate Zones. Geographies 3, 477–498.

Santos, P.P., Pereira, S., Zêzere, J.L., Reis, E., Oliveira, S.C., Garcia, R.A.C., Ferreira, T.M., 2025. Understanding flood risk in urban environments: spatial analysis of building vulnerability and hazard areas in the Lisbon metropolitan area. Nat. Hazards 121, 23603–23626.

Sathianarayanan, M., Hsu, P.-H., 2026. The impact of Köppen–Geiger climate transitions and land cover changes on natural hazards in Taiwan. J. Water Clim. Chang.

Sathianarayanan, M., Hsu, P.H., 2023. SPATIAL DOWNSCALING OF GPM IMERG V06 GRIDDED PRECIPITATION USING MACHINE LEARNING ALGORITHMS. Int. Arch. Photogramm. Remote Sens. Spatial Inf. Sci. XLVIII-4/W6-2022, 327–332.

Tsou, C.-Y., Feng, Z.-Y., Chigira, M., 2011. Catastrophic landslide induced by Typhoon Morakot, Shiaolin, Taiwan. Geomorphology 127, 166–178.

Vuillez, C., Tonini, M., Sudmeier-Rieux, K., Devkota, S., Derron, M.-H., Jaboyedoff, M., 2018. Land use changes, landslides and roads in the Phewa Watershed, Western Nepal from 1979 to 2016. Applied Geography 94, 30–40.

Yang, T.-H., Yang, S.-C., Ho, J.-Y., Lin, G.-F., Hwang, G.-D., Lee, C.-S., 2015. Flash flood warnings using the ensemble precipitation forecasting technique: A case study on forecasting floods in Taiwan caused by typhoons. J. Hydrol. 520, 367–378.

Yilmaz, A.G., 2016. Climate change effects and extreme rainfall non-stationarity. Proceedings of the Institution of Civil Engineers - Water Management 170, 57–65.